Ultrafast Laser-Induced Formation of Hollow Gold Nanorods and Their Optical Properties

Yong Gan,* Hao Cai, and Chang Niu

ACCESS | Metrics & More | Article Recommendations | Supporting Information

ABSTRACT: Laser irradiation has been shown to be an efficient means to modify structures and shapes of plasmonic nanoparticles for tuning their properties. Thermomechanical deformations of single-crystal and penta-twinned gold nanorods by femtosecond laser irradiations have been studied by classical molecular dynamics simulations. It is demonstrated that hollow gold nanorods could be formed by femtosecond laser irradiations under certain conditions of maximum temperatures in nanorods by laser heating and cooling rates due to the extrinsic solvent. For a given maximum temperature and cooling rate, a larger cavity is induced in the irradiated single-crystal nanorod. The results also indicate that at the same cooling rate a higher threshold of maximum temperature can be required for producing the cavity in the twinned nanorod. The optical spectra of the laser-irradiated gold nanorods are calculated, and the shifts in the surface plasmon resonance peak of the nanorods are illustrated due to the thermal reshaping and the plasmon hybridization mechanism. Moreover, we show the formation of the hollow gold nanorod possessing the surface plasmon resonance peak in the second near-infrared window and a relatively small aspect ratio (~2.8), which is highly desirable and suitable for serving as agents in biomedical imaging and photothermal therapy applications.
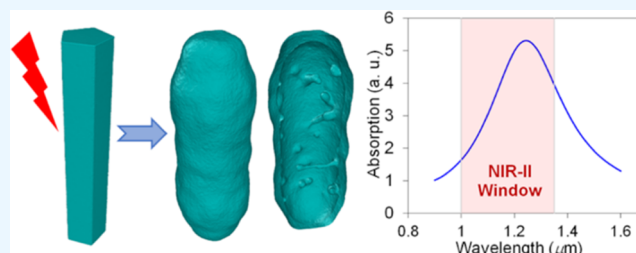
1. INTRODUCTION

Noble-metal nanoparticles are one of the important materials at nanoscale due to their exceptional chemical, plasmonic, and biocompatible properties and great potential in the fields such as catalysis, photonics, sensing and imaging, biomedical diagnosis and therapy.[1−8] As compared to solid counterparts, hollow nanoparticles possess lower density, higher surface-area-to-volume ratio, and enhanced properties,[9,10] which stimulates an increasing interest in hollow noble-metal nanoparticles and many efforts to develop the methods to prepare hollow noble-metal nanoparticles. So far, the fabrications of hollow nanoparticles by template-mediated techniques, metal diffusion based on the Kirkendall effect, and the galvanic replacement method have been reported.[11−14] In addition to chemical synthesis methods, laser irradiation has recently attracted increasing attention as an effective and flexible means for the production of hollow nanoparticles.[15−18] For example, it was demonstrated that nanosecond laser irradiation can lead to the formation of hollow gold nanoparticles, and hollow metal nanospheres were fabricated by pulsed-laser selective heating of colloidal nanoparticles.[15,16]

It is worth noting that all existing studies mainly discussed the laser production of symmetrically shaped hollow nanospheres. Compared with spherical nanoparticles, rodlike noble-metal nanoparticles provide optical anisotropies and show better performances in the applications illustrated with nanospheres.[19−21] For instance, gold nanorods are a more advantageous agent with tunable optical response to lights in the near-infrared (NIR) wavelength region for biomedical imagining, drug delivery, and thermotherapy.[22−25] As a result, it is of great necessity and interest to investigate the formation process and properties of hollow noble-metal nanorods by laser irradiation, both from a fundamental point of view of understanding the effects of particle shapes and structures on the production of hollow nanoparticles and from an applied viewpoint for the use of hollow noble-metal nanorods in the applications such as biomedicine and energy storage.

Among nanoparticles for different noble-metal elements, gold nanoparticles are of particular interest for their unique physical and chemical properties. Here, we report the classical molecular dynamics (MD) simulations of thermomechanical deformations of single-crystal and penta-twinned gold nanorods by ultrafast laser irradiations, with the consideration of heat dissipations due to the solvent environments. The simulations show that the empty cavity can be formed in the nanorods by ultrafast laser irradiations under certain conditions of maximum temperatures in nanorods and cooling rates. With the same chosen cooling rates, a higher threshold of
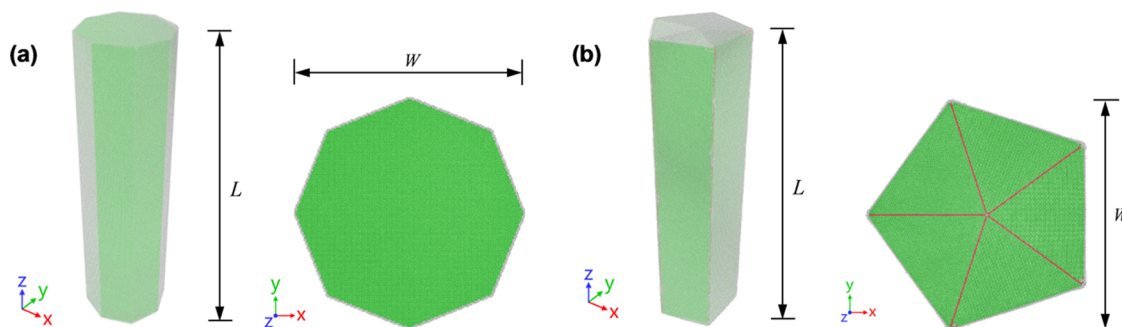
Figure 1. MD models of the considered (a) single-crystal and (b) penta-twinned solid gold nanorods. The nanorods are half-cut normal to the long rod axis to show the cross sections and the internal crystal structures. The fcc, hcp, and disordered atoms are colored green, red, and white, respectively.
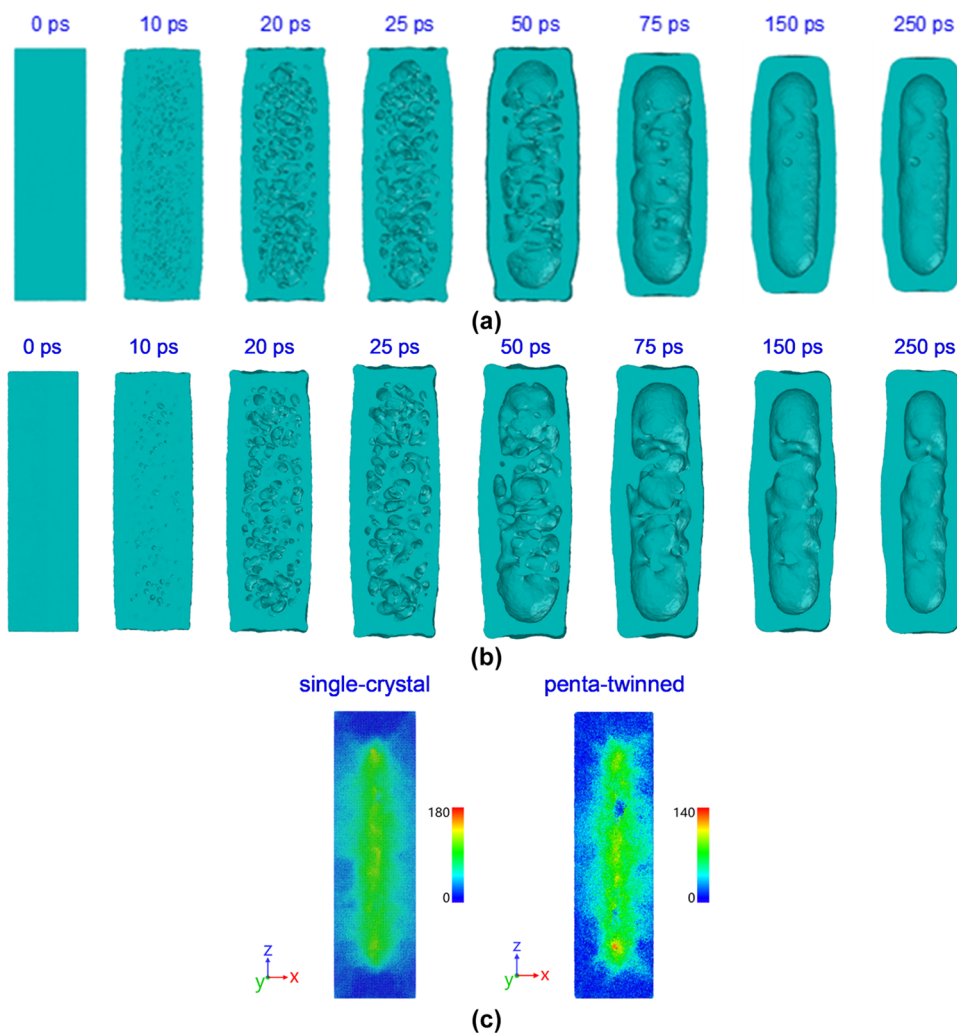

Figure 2. Atomic snapshots of (a) single-crystal and (b) penta-twinned gold nanorods irradiated by femtosecond lasers at different times. (c) Initial atomic snapshots of single-crystal and penta-twinned gold nanorods. In (c), the nanorods are half-cut and the unit of color legend is Å.

maximum temperature is required to induce the formation of a cavity in the penta-twinned gold nanorod. It is also revealed that for the same cooling rate and maximum temperature in nanorod, the volume of the cavity in the laser-irradiated single-crystal nanorod is larger than that in the irradiated twinned nanorod, which can be attributed to the different cross-section shapes of the single-crystal and twinned nanorods. The optical spectra of the laser-irradiated gold nanorods are calculated based on the corresponding final MD atomistic configurations.

The shifts of the surface plasmon resonance (SPR) band of the heated gold nanorods are exhibited due to the thermal reshaping and the plasmon hybridization mechanism. Particularly, we demonstrate the formation of the hollow gold nanorod possessing a longitudinal plasmon band in the second NIR window as well as relatively small size (less than 200 nm) and aspect ratio (~2.8), which is highly desirable and suitable for serving as agents in the biomedical imaging and photothermal therapy applications.

2. METHOD AND MODEL

The MD simulations on femtosecond laser irradiations of solid gold nanorods in solvent are conducted using the simulation tool of LAMMPS.[26] Figure 1 shows the atomistic MD models of single-crystal and penta-twinned solid gold nanorods considered, both having a width $W = 30$ nm and an aspect ratio $L/W = 3.5$. The single-crystal nanorod as illustrated in Figure 1a has eight high-index {250} side facets parallel to the growth direction of [001] and two {001} end facets.[27] In the penta-twinned nanorod as shown in Figure 1b, five {100} side facets are oriented along the [110] growth direction of the nanorod and two {100} facets are located at the rod ends.[28,29]

The femtosecond laser heating of nanorods is mimicked by linearly increasing the lattice temperature from room temperature of 298 K to a maximum value T_{max} between 2000 and 4000 K in the microcanonical ensemble within 7 ps.[16] The rapid cooling of gold nanorods due to the dissipation of heat from hot nanorods to the surrounding solvent is modeled by applying a Langevin thermostat in the MD,[16,30] which simulates the interactions of atoms with a background implicit solvent. Different damping parameters of $\tau = 60$, 120, and 350 ps are used for the Langevin thermostat to describe the rates for cooling the nanorods in various environmental conditions. The smaller the damping parameter τ, the faster the cooling of hot nanorods. An aqueous environment can be represented by the damping parameter $\tau = 60$ ps,[31] while $\tau = 350$ ps corresponds to the CTAB-capped gold nanorod at the critical micelle concentration.[32] By following ref 16, the value of $\tau = 120$ ps is employed to consider the intermediate heat dissipation condition. Throughout all MD simulations, the free boundary condition is applied along all directions and a time step of 2.5 fs is used. The interatomic interactions between atoms in the gold nanorods are described using the embedded-atom method (EAM) potential for gold in ref 33. Total simulation times are ~375 ps, ~625 ps, and ~1.5 ns for the cases of $\tau = 60$, 120, and 350 ps, respectively. Prior to the MD simulations for femtosecond laser irradiations of nanorods, the MD models of nanorods are thermally relaxed at room temperature 298 K for 1 ns in the canonical using the Nose−Hoover thermostatting algorithm.[34]

The optical spectra of gold nanorods in a water medium are calculated using the discrete dipole approximation (DDA) method considering two orthogonal polarizations of the incident radiation.[35] The models for DDA calculation are developed from the final MD atomistic configurations of laser-irradiated gold nanorods by the following two steps. First, the triangulated surface meshes for the final MD atomistic configuration of laser-irradiated nanorods are constructed. Second, the DDA calculation model consisting of an array of dipole points within the space defined by the constructed surface meshes is generated via the tools of DDSCAT Convert or Atomsk.[36,37] For each DDA model, there are more than 50 000 dipole points to ensure computational accuracy. In all DDA calculations, the values of the complex dielectric function of gold at various wavelengths proposed by Johnson and Christy are used with the corrections for nanoparticles and the water has a refractive index of $1.33 + 0i$.[38,39]

3. RESULTS AND DISCUSSION

We first present the transient structural transformations of gold nanorods induced by femtosecond laser irradiations. Figure 2a,b shows the atomistic snapshots of the laser-irradiated single-crystal and twinned gold nanorods at different times for the case of $T_{max} = 3000$ K and $\tau = 60$ ps, respectively, in which the nanorods are half-cut and the surface mesh is constructed to better visualize the voids and cavities in the nanorods. At the early time of 10 ps, small voids in the nanorods can be clearly observed. With the evolution of time, a growing number of voids with larger volumes are shown (20 and 25 ps) and merge into a big cavity (50 and 75 ps), and finally stable hollow gold nanorods are formed. This structural deformation pattern for gold nanorods is quite similar to that in femtosecond laser ablation of metallic targets as previously demonstrated by MD.[40] Femtosecond laser irradiation induces not only the melting of nanorods but also the building up of high compressive stress in the nanorods at the early time, as illustrated in Figure S1. The unloading tensile stress by the relaxation of the laser-induced compression leads to the expansion of the melt, forming the cavities inside the nanorods. Due to the sufficiently fast cooling, the melted nanorods are resolidified with the preserved cavity, leading to the production of hollow gold nanorods. During the formation of hollow nanorods, the atoms in the core region of nanorods undergo more significant displacements, as shown in Figure 2c of the initial atomic snapshots of nanorods, where the atoms are colored with the displacement magnitudes obtained by the subtraction of the initial position vectors of atoms from those at 250 ps.

Figure 3 illustrates the snapshots for the final MD atomistic configurations of gold nanorods irradiated by femtosecond lasers for different values of T_{max} and τ. At a slow cooling rate with $\tau = 350$ ps, no hollow nanorods are formed (see Figure S2) because the molten nanorods with an inner cavity have sufficient time to eventually transform into thermodynamically stable solid particles before the melt is resolidified. As the cooling rates are increased using smaller damping time values of $\tau = 60$ and 120 ps, the hollow nanorods are produced for the maximum temperatures above 2500 K. It is observed that the maximum temperature of 2000 K is too low to form hollow gold nanorods, even for the adopted highest cooling rate with $\tau = 60$ ps. As displayed in Figure 3, when the maximum temperature of 2500 K is used, the empty cavities are eventually preserved in the laser-irradiated single-crystal and twinned gold nanorod for the highest cooling rate of $\tau = 60$ ps; moreover, only two very tiny voids are present in the end regions of the laser-heated twinned nanorod for the cooling rate of $\tau = 60$ ps. It can thus be inferred that at damping time $\tau = 60$ ps, a higher threshold of maximum temperature is required to induce the formation of a cavity in the penta-twinned gold nanorod. This suggests that in addition to the maximum temperature and cooling rate, the original nanoparticle structure and geometry are also key factors for the occurrence of cavity formation in nanoparticles by femtosecond laser irradiation.

We further examine the volumes of the cavity in the laser-irradiated gold nanorods. For this, the triangulated surface meshes are constructed to geometrically describe the inner and outer surfaces of the final MD atomistic configurations of the irradiated nanorods, and the volume of the empty space enclosed by the inner surface mesh is calculated and set as the volume of the cavity inside the nanorods. Figure 4 compares the volumes of the cavity inside the laser-irradiated gold nanorods at the cooling rates of $\tau = 60$ and 120 ps. As expected, the cavity volume increases with the increase of the maximum temperature T_{max} for a given cooling rate, and a
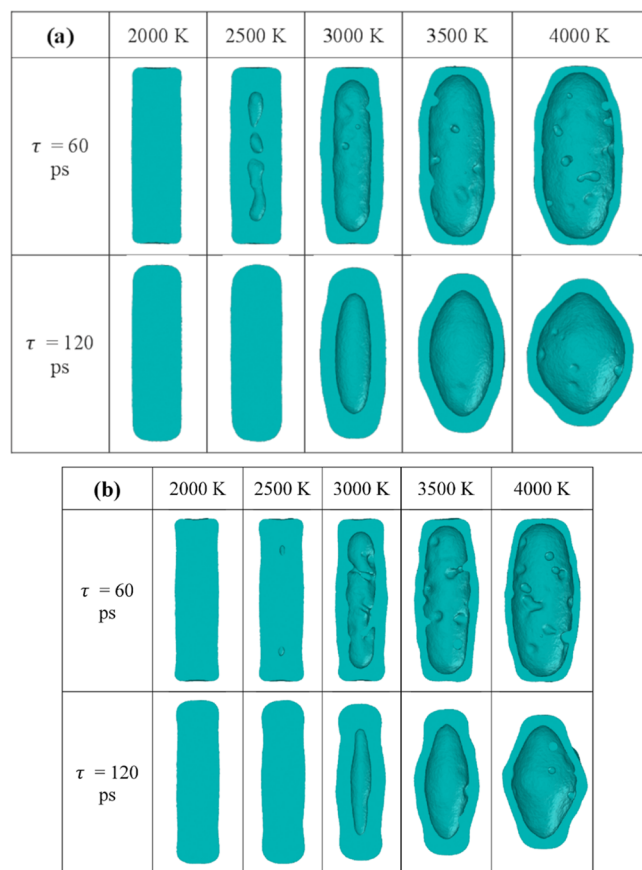
Figure 3. Snapshots of the final MD configurations of the laser-irradiated gold nanorods for different values of T_{max} and τ: (a) single-crystal gold nanorod and (b) penta-twinned gold nanorod. The nanorods are half-cut and the surface mesh is built for clear visualization of the cavity.

Figure 5. Atomic snapshots for the cross sections of laser-irradiated (a) single-crystal and (b) penta-twinned gold nanorods at time 7.5 ps. The corresponding temperatures of nanorods at 7.5 ps are given below the figures.

higher cooling rate yields a larger cavity in the gold nanorods for a given T_{max}. With the same T_{max} and τ, the volumes of the cavity in the irradiated twinned nanorods are smaller than those in the irradiated single-crystal nanorods. It should be noted that the gold nanorods studied here have different crystalline structures and geometrical shapes. Meanwhile, we notice that the generation of an empty cavity inside gold nanorods is attributed to the expansion of the melt and that at the beginning of the melt expansion, the cross-section shapes of the melted nanorods are similar to the initial ones, as shown in Figure 5. Therefore, the discrepancies in the volumes of the
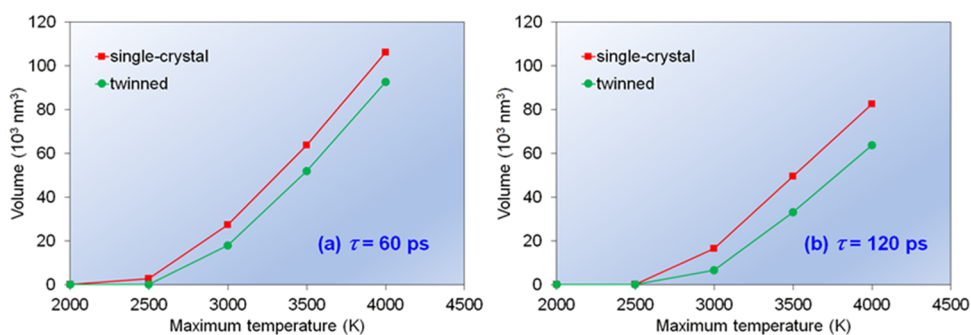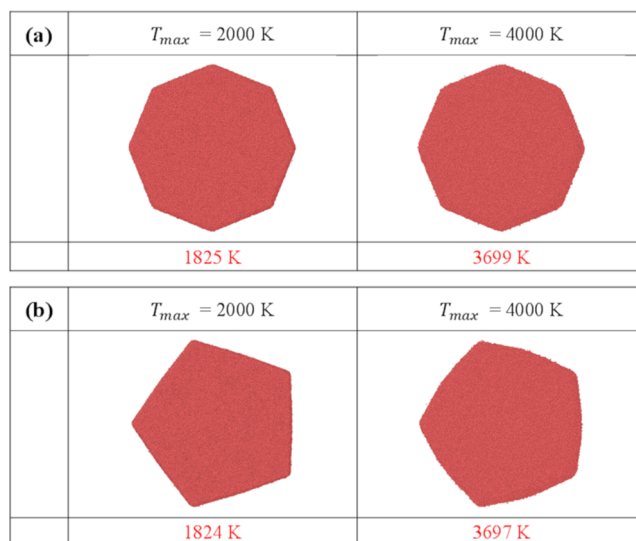
cavity within laser-irradiated nanorods as observed in Figure 4 are very likely due to the different cross-section shapes of nanorods. To illustrate this, we have performed the MD simulations for femtosecond laser irradiations of the single-crystal gold nanorod that has the [001] long axis and the same sizes and pentagon cross section as those of the penta-twinned nanorod, as shown in Figure S3. It is found that the volumes of the cavity in the laser-heated single-crystal and twinned nanorods with the same pentagon cross section are close (see Figure S4), confirming the role of the nanorod cross-section shape in the formation of a cavity inside the nanorods. Likewise, the aforementioned different thresholds of maximum temperature T_{max} for the formation of a cavity in the laser-irradiated nanorods for τ = 60 ps can also be ascribed to the difference in the cross-section shapes of nanorods.

In addition to the formation of a cavity, gold nanorods under femtosecond laser irradiation will also undergo thermal reshaping, as illustrated in Figure S5 for the aspect ratios of laser-irradiated nanorods. At a given cooling rate, a smaller aspect ratio of nanorods is induced using a higher maximum temperature. It has been demonstrated that the diminishing aspect ratio of the nanorod is associated with the blue-shift of the longitudinal SPR band of nanorod.[27,41] On the other hand,

Figure 4. Comparisons of the volumes of the cavity in the femtosecond laser-irradiated gold nanorods for different values of T_{max} and τ: (a) single-crystal gold nanorods and (b) penta-twinned gold nanorods.

according to the plasmon hybridization model,[42] the plasmon response of hollow nanoparticles can be viewed as the interaction between particle and cavity plasmons. The strength of this interaction is dependent on the thickness of the shell layer of hollow particles. The plasmon energy is red shifted as the shell thickness is reduced.[42] Therefore, thermal reshaping and plasmon hybridization are two competing mechanisms for the shifts of the longitudinal SPR band of hollow gold nanorods.

Figure 6a shows the calculated absorption spectra of the laser-irradiated single-crystal gold nanorods in an embedded
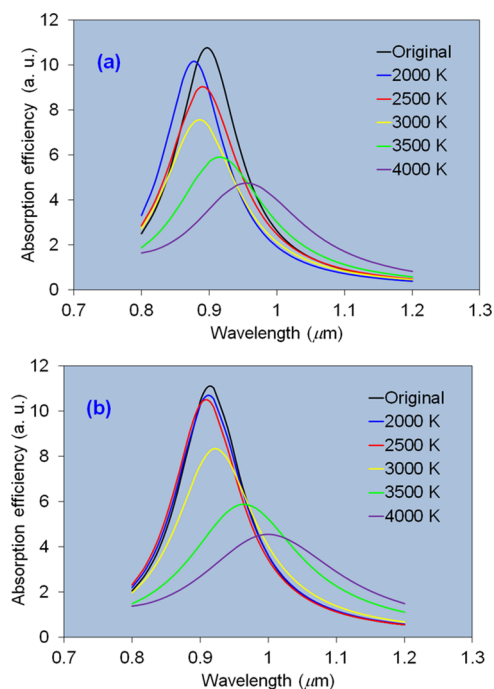

Figure 6. Calculated absorption spectra of the ultrafast laser-irradiated (a) single-crystal and (b) twinned gold nanorods in water for different maximum temperatures.

water medium for the cooling rate of τ = 60 ps. For the purpose of comparison, the absorption spectrum of the original gold nanorod in water is also included in the figure. The results reveal that the nanorods irradiated with the maximum

temperatures of 2000, 2500, and 3000 K show a blue-shift of the longitudinal SPR wavelength. At T_{max} = 2000 K, no cavity is formed in the nanorod and the observed blue-shift is consistent with the decreased aspect ratio through thermal reshaping as shown in Figure S5a. At higher T_{max} of 2500 and 3000 K, the cavity inside the nanorods is produced, along with the further decreased aspect ratio of nanorods. The blue-shifts of the SPR peak at T_{max} = 2500 and 3000 K suggest that the plasmon hybridization mechanism is surpassed by the thermal reshaping effect for the optical responses of the formed hollow nanorods. As the maximum temperature increases to 3500 and 4000 K, the cavity volume is further increased and consequently, the shell layer of hollow nanorods gets thinner. Thus, the interaction between particle and cavity plasmons becomes stronger and plays a dominant role in the plasmonic responses of hollow nanorods, leading to the red-shifts of the SPR band of hollow gold nanorods as shown in Figure 6a.

The corresponding calculated absorption spectra of the laser-irradiated twinned gold nanorods in water are shown in Figure 6b. For low T_{max} of 2000 and 2500 K, very small blue-shifts of the longitudinal SPR wavelength of the nanorods are shown. As the maximum temperature is increased from 3000 to 4000 K, the longitudinal SPR band is continuously red shifted due to the increasing strength of the interaction between particle and cavity plasmons. In particular, for the laser irradiation with T_{max} of 4000 K, the longitudinal SPR wavelength of the nanorod is distinctly red shifted to ∼1000 nm and the hollow nanorod is found to have a length of ∼108 nm and an aspect ratio of ∼2.1. Stimulated by this observation, we further simulated the ultrafast laser irradiation of the penta-twinned gold nanorod with a higher aspect ratio of 5 and the same width using the parameters of T_{max} = 4000 K and τ = 60 ps. Figure 7 shows the final atomistic snapshot and the calculated absorption spectrum of the formed hollow nanorod, which has a length of ∼145 nm and an aspect ratio of ∼2.8. Moreover, the longitudinal SPR wavelength of this hollow nanorod is found to be ∼1240 nm.

It is known that the second NIR window of 1000−1350 nm is more suitable for biological and biomedical applications than the first NIR window of 650−950 nm due to the greatly improved signal-to-noise ratio and tissue penetration depth.[43] Conventional solid gold nanorods with strong optical responses in the second NIR window usually have large aspect ratios or dimensions and are unfavorable for biomedical
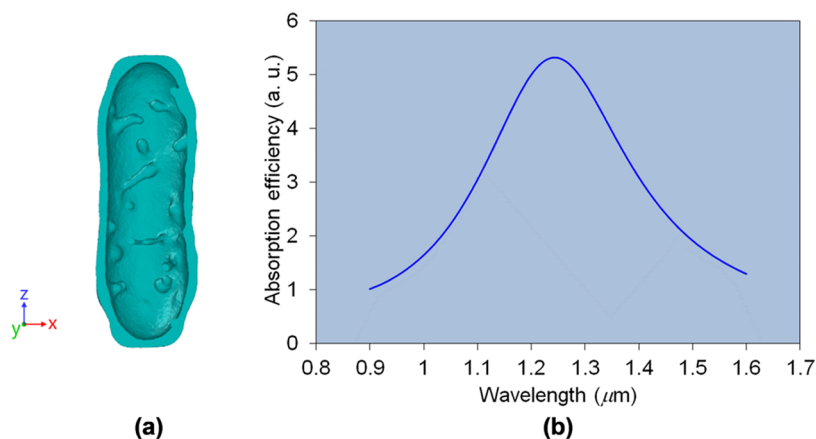

Figure 7. (a) Snapshot for the final MD configuration and (b) absorption spectrum of the hollow gold nanorod produced by the ultrafast laser irradiation of the penta-twinned gold nanorod of the initial W = 30 nm and aspect ratio L/W = 5 with T_{max} = 4000 K and τ = 60 ps.

applications owing to the resulting low thermal stability and tissue penetration rate, short half-lives in blood, and poor extravasation.[22] For example, nanoparticles larger than 200 nm are inappropriate for in vivo applications since they can accumulate in the liver and spleen through intravenous injection.[44] Therefore, the above as-formed hollow gold nanorod with the SPR peak in the second NIR window and relatively small size (less than 200 nm) and aspect ratio (~2.8) is well suited to serve as agents for biomedical sensing, imaging, and photothermal therapy applications.[11,44]

4. CONCLUSIONS

In summary, thermomechanical deformations of single-crystal and penta-twinned gold nanorods induced by ultrafast laser irradiations have been simulated using the MD method with the consideration of the cooling of nanorods due to the surrounding solvent. It is illustrated that ultrafast laser irradiation can lead to the formation of a cavity in gold nanorods under certain conditions of maximum temperatures in nanorods and cooling rates. For a given maximum temperature and cooling rate, a larger cavity is produced in the irradiated single-crystal nanorod. Such discrepancies in the volumes of the cavity in laser-irradiated gold nanorods can be attributed to the different cross-section shapes of the nanorods. The results also show that at the same chosen cooling rate a higher threshold of maximum temperature can be required for producing the cavity in the twinned nanorod. The optical spectra of the laser-irradiated gold nanorods are calculated with the corresponding final MD atomistic configurations and the DDA method. The blue- and red-shifts in the longitudinal SPR wavelength of the laser-heated gold nanorods are shown due to the thermal reshaping effect and the plasmon hybridization mechanism. Moreover, the production of the hollow gold nanorod with the longitudinal SPR band in the second NIR window and relatively small size and aspect ratio is demonstrated, which is exceedingly desirable and suitable for serving as agents in the biomedical in vivo applications of imaging and photothermal therapy.

■ ASSOCIATED CONTENT

Ⓢ Supporting Information

The Supporting Information is available free of charge at https://pubs.acs.org/doi/10.1021/acsomega.2c05436.

> Time histories of pressure in the gold nanorods irradiated by femtosecond laser with T_{max} = 3000 K and τ = 60 ps; snapshots of the final MD configurations of the laser-irradiated gold nanorods for T_{max} = 4000 K and τ = 350 ps; MD model of the considered single-crystal nanorod with the [001] long axis and the same pentagon cross section as that of the twinned nanorod; the volumes of the cavity in the single-crystal and twinned nanorods with the same pentagon cross section for different values of T_{max}; and the aspect ratios of the ultrafast laser-irradiated gold nanorods for different values of T_{max} (PDF)

■ AUTHOR INFORMATION

Corresponding Author

Yong Gan − School of Aeronautics and Astronautics, Faculty of Engineering, Key Laboratory of Soft Machines and Smart Devices of Zhejiang Province, Zhejiang University, Hangzhou 310027 Zhejiang, China; ● orcid.org/0000-0002-5105-1989; Email: ganyong@zju.edu.cn

Authors

Hao Cai − School of Aeronautics and Astronautics, Faculty of Engineering, Key Laboratory of Soft Machines and Smart Devices of Zhejiang Province, Zhejiang University, Hangzhou 310027 Zhejiang, China

Chang Niu − School of Aeronautics and Astronautics, Faculty of Engineering, Key Laboratory of Soft Machines and Smart Devices of Zhejiang Province, Zhejiang University, Hangzhou 310027 Zhejiang, China

Complete contact information is available at:
https://pubs.acs.org/10.1021/acsomega.2c05436

Notes

The authors declare no competing financial interest.

■ REFERENCES

(1) Huang, X.; Neretina, S.; El-Sayed, M. A. Gold Nanorods: From Synthesis and Properties to Biological and Biomedical Applications. *Adv. Mater.* **2009**, *21*, 4880−4910.

(2) Wu, Y.; Ali, M. R. K.; Chen, K.; Fang, N.; El-Sayed, M. A. Gold Nanoparticles in Biological Optical Imaging. *Nano Today* **2019**, *24*, 120−140.

(3) Saha, K.; Agasti, S. S.; Kim, C.; Li, X.; Rotello, V. M. Gold Nanoparticles in Chemical and Biological Sensing. *Chem. Rev.* **2012**, *112*, 2739−2779.

(4) Lee, K.-S.; El-Sayed, M. A. Gold and Silver Nanoparticles in Sensing and Imaging: Sensitivity of Plasmon Response to Size, Shape, and Metal Composition. *J. Phys. Chem. B* **2006**, *110*, 19220−19225.

(5) Daraee, H.; Eatemadi, A.; Abbasi, E.; Fekri Aval, S.; Kouhi, M.; Akbarzadeh, A. Application of Gold Nanoparticles in Biomedical and Drug Delivery. *Artif. Cells Nanomed. Biotechnol.* **2016**, *44*, 410−422.

(6) Sharifi, M.; Attar, F.; Saboury, A. A.; Akhtari, K.; Hooshmand, N.; Hasan, A.; El-Sayed, M. A.; Falahat, M. Plasmonic Gold Nanoparticles: Optical Manipulation, Imaging, Drug Delivery and Therapy. *J. Controlled Release* **2019**, *311−312*, 170−189.

(7) Elahi, N.; Kamali, M.; Baghersad, M. H. Recent Biomedical Applications of Gold Nanoparticles: A Review. *Talanta* **2018**, *184*, 537−556.

(8) Yang, X.; Yang, M.; Pang, B.; Vara, M.; Xia, Y. Gold Nanomaterials at Work in Biomedicine. *Chem. Rev.* **2015**, *115*, 10410−10488.

(9) Jiang, L.; Yin, X.; Zhao, J.; Liu, H.; Liu, Y.; Wang, F.; Zhu, J.; Boey, F.; Zhang, H. Theoretical Investigation on the Thermal Stability of Hollow Gold Nanoparticles. *J. Phys. Chem. C* **2009**, *113*, 20193−20197.

(10) Valencia, F. J.; Ramírez, M.; Varas, A.; Rogan, J. Thermal Sensitivity on Eccentric Gold Hollow Nanoparticles: A Perspective from Atomistic Simulations. *J. Chem. Inf. Model.* **2021**, *61*, 5499−5507.

(11) Cai, K.; Zhang, W.; Foda, M. F.; Li, X.; Zhang, J.; Zhong, Y.; Liang, H.; Li, H.; Han, H.; Zhai, T. Miniature Hollow Gold Nanorods with Enhanced Effect for In Vivo Photoacoustic Imaging in the NIR-II Window. *Small* **2020**, *16*, No. 2002748.

(12) Ben Moshe, A.; Markovich, G. Synthesis of Single Crystal Hollow Silver Nanoparticles in a Fast Reaction-Diffusion Process. *Chem. Mater.* **2011**, *23*, 1239−1245.

(13) Yu, L.; Yu, X. Y.; Lou, X. W. The Design and Synthesis of Hollow Micro-/Nanostructures: Present and Future Trends. *Adv. Mater.* **2018**, *30*, No. 1800939.

(14) Dung, N. T.; Linh, N. T. N.; Chi, D. L.; Hoa, N. T. H.; Hung, N. P.; Ha, N. T.; Nam, P. H.; Phuc, N. X.; Tam, L. T.; Lu, L. T. Optical Properties and Stability of Small Hollow Gold Nanoparticles. *RSC Adv.* **2021**, *11*, 13458−13465.

(15) González-Rubio, G.; Milagres de Oliveira, T.; Albrecht, W.; Díaz-Núñez, P.; Castro-Palacio, J. C.; Prada, A.; González, R. I.; Scarabelli, L.; Bañares, L.; Rivera, A.; Liz-Marzán, L. M.; Peña-Rodríguez, O.; Bals, S.; Guerrero-Martínez, A. Formation of Hollow Gold Nanocrystals by Nanosecond Laser Irradiation. *J. Phys. Chem. Lett.* **2020**, *11*, 670−677.

(16) Castro-Palacio, J. C.; Ladutenko, K.; Prada, A.; González-Rubio, G.; Díaz-Núñez, P.; Guerrero-Martínez, A.; Fernández de Córdoba, P.; Kohanoff, J.; Perlado, J. M.; Peña-Rodríguez, O.; Rivera, A. Hollow Gold Nanoparticles Produced by Femtosecond Laser Irradiation. *J. Phys. Chem. Lett.* **2020**, *11*, 5108−5114.

(17) Jiang, C.; Mo, Y.; Wang, H.; Li, R.; Huang, M.; Jiang, S. Molecular Dynamics Simulation of the Production of Hollow Silver Nanoparticles under Ultrafast Laser Irradiation. *Comput. Mater. Sci.* **2021**, *196*, No. 110545.

(18) Arce, V. B.; JMJ Santillan, J. M. J.; Arboleda, D. M.; Muraca, D.; Scaffardi, L. B.; Schinca, D. C. Characterization and Stability of Silver Nanoparticles in Starch Solution Obtained by Femtosecond Laser Ablation and Salt Reduction. *J. Phys. Chem. C* **2017**, *121*, 10501−10513.

(19) Oldenburg, A. L.; Hansen, M. N.; Zweifel, D. A.; Wei, A.; Boppart, S. A. Plasmon-Resonant Gold Nanorods as Low Backscattering Albedo Contrast Agents for Optical Coherence Tomography. *Opt. Express* **2006**, *14*, 6724−6738.

(20) Wang, H.; Huff, T. B.; Zweifel, D. A.; He, W.; Low, P. S.; Wei, A.; Cheng, J.-X. In Vitro and In Vivo Two-Photon Luminescence Imaging of Single Gold Nanorods. *Proc. Natl. Acad. Sci. U.S.A.* **2005**, *102*, 15752−15756.

(21) Li, W.; Chen, X. Gold Nanoparticles for Photoacoustic Imaging. *Nanomedicine* **2015**, *10*, 299−320.

(22) Chen, Y.-S.; Zhao, Y.; Yoon, S. J.; Gambhir, S. S.; Emelianov, S. Miniature Gold Nanorods for Photoacoustic Molecular Imaging in the Second Near-Infrared Optical Window. *Nat. Nanotechnol.* **2019**, *14*, 465−472.

(23) Alkilany, A. M.; Thompson, L. B.; Boulos, S. P.; Sisco, P. N.; Murphy, C. J. Gold Nanorods: Their Potential for Photothermal Therapeutics and Drug Delivery, Tempered by the Complexity of Their Biological Interactions. *Adv. Drug Delivery Rev.* **2012**, *64*, 190−199.

(24) Tong, L.; Wei, Q.; Wei, A.; Cheng, J.-X. Gold Nanorods as Contrast Agents for Biological Imaging: Optical Properties, Surface Conjugation and Photothermal Effects. *Photochem. Photobiol.* **2009**, *85*, 21−32.

(25) Kuo, W.-S.; Chang, C.-N.; Chang, Y.-T.; Yang, M.-H.; Chien, Y.-H.; Chen, S.-J.; Yeh, C.-S. Gold Nanorods in Photodynamic Therapy, as Hyperthermia Agents, and in Near-Infrared Optical Imaging. *Angew. Chem., Int. Ed.* **2010**, *49*, 2711−2715.

(26) Thompson, A. P.; Aktulga, H. M.; Berger, R.; Bolintineanu, D. S.; Brown, W. M.; Crozier, P. S.; in't Veld, P. J.; Kohlmeyer, A.; Moore, S. G.; Nguyen, T. D.; Shan, R.; Stevens, M. J.; Tranchida, J.; Trott, C.; Plimpton, S. J. LAMMPS - a Flexible Simulation Tool for Particle-Based Materials Modeling at the Atomic, Meso, and Continuum Scales. *Comput. Phys. Commun.* **2022**, *271*, No. 108171.

(27) Carbó-Argibay, E.; Rodríguez-González, B.; Gómez-Graña, S.; Guerrero-Martínez, A.; Pastoriza-Santos, I.; Pérez-Juste, J.; Liz-Marzán, L. M. The Crystalline Structure of Gold Nanorods Revisited: Evidence for Higher-Index Lateral Facets. *Angew. Chem., Int. Ed.* **2010**, *49*, 9397−9400.

(28) Hu, M.; Hillyard, P.; Hartland, G. V.; Kosel, T.; Perez-Juste, J.; Mulvaney, P. Determination of the Elastic Constants of Gold Nanorods Produced by Seed Mediated Growth. *Nano Lett.* **2004**, *4*, 2493−2497.

(29) Petrova, H.; Perez-Juste, J.; Zhang, Z.; Zhang, J.; Kosel, T.; Hartland, G. V. Crystal Structure Dependence of the Elastic Constants of Gold Nanorods. *J. Mater. Chem.* **2006**, *16*, 3957−3963.

(30) Schneider, T.; Stoll, E. Molecular-Dynamics Study of a Three-Dimensional One-Component Model for Distortive Phase Transitions. *Phys. Rev. B* **1978**, *17*, 1302.

(31) Ekici, O.; Harrison, R. K.; Durr, N. J.; Eversole, D. S.; Lee, M.; Ben-Yakar, A. Thermal Analysis of Gold Nanorods Heated with Femtosecond Laser Pulses. *J. Phys. D: Appl. Phys.* **2008**, *41*, No. 185501.

(32) Nguyen, S. C.; Zhang, Q.; Manthiram, K.; Ye, X.; Lomont, J. P.; Harris, C. B.; Weller, H.; Alivisatos, A. P. Study of Heat Transfer Dynamics from Gold Nanorods to the Environment via Time-Resolved Infrared Spectroscopy. *ACS Nano* **2016**, *10*, 2144−2151.

(33) Sheng, H. W.; Kramer, M. J.; Cadien, A.; Fujita, T.; Chen, M. W. Highly Optimized Embedded-Atom-Method Potentials for Fourteen FCC Metals. *Phys. Rev. B* **2011**, *83*, No. 134118.

(34) Shinoda, W.; Shiga, M.; Mikami, M. Rapid Estimation of Elastic Constants by Molecular Dynamics Simulation under Constant Stress. *Phys. Rev. B* **2004**, *69*, No. 134103.

(35) Draine, B. T.; Flatau, P. J. Discrete-Dipole Approximation for Scattering Calculations. *J. Opt. Soc. Am. A* **1994**, *11*, 1491−1499.

(36) Feser, J.; Sobh, A. R.; nanoHUB. DDSCAT Convert: A Target Generation Tool, 2019. https://nanohub.org/resources/ddaconvert.

(37) Hirel, P. Atomsk: A Tool for Manipulating and Converting Atomic Data Files. *Comput. Phys. Commun.* **2015**, *197*, 212−219.

(38) Johnson, P. B.; Christy, R. W. Optical Constants of the Noble Metals. *Phys. Rev. B* **1972**, *6*, 4370−4379.

(39) Derkachova, A.; Kolwas, K.; Demchenko, I. Dielectric Function for Gold in Plasmonics Applications: Size Dependence of Plasmon Resonance Frequencies and Damping Rates for Nanospheres. *Plasmonics* **2016**, *11*, 941−951.

(40) Starikov, S. V.; Pisarev, V. V. Atomistic Simulation of Laser-Pulse Surface Modification: Predictions of Models with Various Length and Time Scales. *J. Appl. Phys.* **2015**, *117*, No. 135901.

(41) Liu, Y.; Mills, E. N.; Composto, R. J. Tuning Optical Properties of Gold Nanorods in Polymer Films through Thermal Reshaping. *J. Mater. Chem.* **2009**, *19*, 2704−2709.

(42) Prodan, E.; Radloff, C.; Halas, N. J.; Nordlander, P. A Hybridization Model for the Plasmon Response of Complex Nanostructures. *Science* **2003**, *302*, 419−422.

(43) Antaris, A. L.; Chen, H.; Cheng, K.; Sun, Y.; Hong, G.; Qu, C.; Diao, S.; Deng, Z.; Hu, X.; Zhang, B.; Zhang, X.; Yaghi, O. K.; Alamparambil, Z. R.; Hong, X.; Cheng, Z.; Dai, H. A Small-Molecule Dye for NIR-II Imaging. *Nat. Mater.* **2016**, *15*, 235−242.

(44) Blanco, E.; Shen, H.; Ferrari, M. Principles of Nanoparticle Design for Overcoming Biological Barriers to Drug Delivery. *Nat. Biotechnol.* **2015**, *33*, 941−951.

(45) Stukowski, A. Visualization and Analysis of Atomistic Simulation Data with OVITO − the Open Visualization Tool. *Model. Simul. Mater. Sci. Eng.* **2010**, *18*, No. 015012.